PUBLISHED VERSION

Stephen C. Warren-Smith, Alastair Dowler, and Heike Ebendorff-Heidepriem
Soft-glass imaging microstructured optical fibers
Optics Express, 2018; 26(26):33604-33612

Check for updates

Soft-glass imaging microstructured optical fibers

STEPHEN C. WARREN-SMITH,[1,2,*] ALASTAIR DOWLER,[1] AND HEIKE EBENDORFF-HEIDEPRIEM[1,2]

[1]*Institute for Photonics and Advanced Sensing (IPAS) and School of Physical Sciences, The University of Adelaide, Adelaide, South Australia 5005, Australia*
[2]*ARC Centre of Excellence for Nanoscale BioPhotonics (CNBP), The University of Adelaide, Adelaide, South Australia 5005, Australia*
*stephen.warrensmith@adelaide.edu.au

Abstract: We demonstrate the fabrication of multi-core (imaging) microstructured optical fiber via soft-glass preform extrusion through a 3D printed titanium die. The combination of extrusion through 3D printed dies and structured element (capillary) stacking allows for unprecedented control of the optical fiber geometry. We have exploited this to demonstrate a 100 pixel rectangular array imaging microstructured fiber. Due to the high refractive index of the glass used ($n = 1.62$), such a fiber can theoretically have a pixel pitch as small as 1.8 μm. This opens opportunities for ultra-small, high-resolution imaging fibers fabricated from diverse glass types.

1. Introduction

Imaging inside the human body is routinely performed in large diameter organs such as the esophagus, lungs, and bowel, which allows for fast diagnostics and key-hole surgery. There is a technological push to reduce the size of tools for minimally-invasive imaging of smaller cavities inside the body. For example, Olympus produces bronchoscopes based on charge-coupled device (CCD) array imaging with dimensions as small as 3.1 mm.

Imaging with fiber optics is a mature technology, with commercially available options such as leached fiber bundles from Schott Glass, imaging fibers from Fujikura, and plastic imaging fibers from Asahi. For example, imaging fibers from Fujikura are available with outer diameters in the range of 0.5 to 2.0 mm and feature between several thousand and up to 100,000 pixels. The limitation of current imaging fibers is that the pitch between cores (pixels) is relatively large (approximately 5 μm or greater) due to the comparatively low index contrast possible with solid-clad fibers. To achieve a high pixel count the outer diameter is large and thus the imaging fiber has limited flexibility.

A scanning fiber endoscope is an alternative configuration in which a single-core optical fiber is scanned mechanically using a piezoelectric actuator to form an image [1]. This can provide video imaging rates with large depth of focus in a 1 mm device. The main limitations of this device are the size of the piezoelectric actuator and the size of packaging required to protect the moving parts (that is, the fiber). An alternative single-core fiber technique is to use multimode fibers for imaging [2,3]. The image information is carried in the different modes of the optical fiber and reconstructed using special pre-calibrated algorithms. This technique can provide relatively high resolution imaging, but is typically restricted to rigid fibers as any bending of the fiber distorts the reconstruction algorithm. The use of advanced computations [4] and the use of graded index multimode fibers [5] have allowed small bends to be supported, though limited to a modest degree of bending. Other recent research trends include using mid-infrared transmitted glass, such as a solid-clad (polymer) chalcogenide fiber bundle [6], albeit with a relatively large diameter of 4 mm.

A design of optical fiber that allows for a large selection in glass, and polymer, materials is the microstructured optical fiber (MOF), which consists of air holes that run along the fiber length [7]. These fibers provide large differences in refractive index, n, in the fiber cross section (e.g. $n = 1.445$ for silica glass and $n = 1.000$ for air). Previous demonstrations to fabricate imaging MOFs have typically focused on polymer fibers. Eijkelenborg demonstrated the fabrication of a 112 core imaging fiber from drilled poly(methyl methacrylate) (PMMA), with an outer diameter of 800 µm [8]. Subsequently, Wang *et al.* fabricated a 547 hole PMMA fiber with 320 µm diameter [9]. However, in this case the attenuation in the polymer fiber limited the length over which an image could be transmitted through the fiber cores to 7-8 cm. Beyond this length capillary guidance allowed coherent image transmission in the holes, due to relatively lower loss compared to the fiber cores. Therefore, while polymer has good compatibility for biomedical use, there is scope for improving the transmission properties of imaging microstructured optical fibers, particularly spectral bandwidth, by using glass as the base material.

The use of glass extrusion to fabricate optical fiber preforms offers opportunities for fabricating complex microstructured optical fibers, such as for imaging. Extrusion allows for a greater degree of freedom in choice of geometry beyond circular features compared to drilling or capillary stacking, particularly for soft-glasses. Examples of fabricating microstructured optical fibers via extrusion include highly asymmetric exposed-core fibers [10] and hollow-core fibers [11]. In 2009 we demonstrated that lead-silicate glass suspended-core fibers can be fabricated with core diameters as small as 420 nm using the extrusion technique for preform fabrication [12]. Such fibers have found applications in sensing, through the significant evanescent field that propagates in the fiber holes [13,14], and nonlinear optics, due to the small optical mode area [15]. We have recently been investigating the use of soft-glass extrusion through 3D printed titanium dies as a method for fabricating microstructured optical fiber preforms [16]. This has great potential for fabricating highly complex optical fiber designs [17,18]. Importantly, we have shown that despite the surface roughness present in 3D printed dies, by simply polishing the exit of the 3D printed die, preforms can be extruded with optical quality surface finish [16]. The fiber structure complexity can also be increased by drawing capillaries from extruded preforms and stacking to form increasingly complex fiber preforms, so-called "structured element stacking" [19,20].

In this paper we demonstrate the versatility of combining extrusion through 3D printed dies and structured element stacking by fabricating a glass-based 100 core imaging microstructured optical fiber, which is effectively an array version of the suspended-core fiber. We then show that theoretically this design can be optimized to allow for greater resolution (that is, greater number of pixels per cross sectional area) than currently possible with conventional imaging fibers due to the high index contrast between glass and air.

2. Fabrication

2.1 Preform extrusion

Titanium extrusion dies were 3D printed with a four core structure suspended by thin struts in a rectangular arrangement. A rectangular arrangement was chosen over a hexagonal arrangement in order to reduce the die complexity (reduced number of bridging struts required) and so that the core alignment can be maintained when stacked. Note that only four cores (2×2 cores) were chosen for this proof-of-concept work in order to reduce the complexity of the extrusion die geometry and gain an understanding of the complex flow behavior of glass through the die, with a view to increasing the number of cores per die in the future. The target geometry, and first die exit tested, is shown in Fig. 1(a). A 30 mm diameter high refractive index lead-silicate glass billet ($n = 1.62$, F2, Schott) was then extruded through the die at relatively high temperature (575°C) and low force (approximately 2,500 N) compared to typical F2 extrusion parameters [21]. This was done to enable better surface

quality, avoid die damage, and reduce die swell. The results of several die iterations are shown in Fig. 1.

When friction exists between the glass and the die wall, as is the case for titanium dies, the phenomenon of die swell is present. This is where an extruded preform will form with larger cross-sectional features compared to the die exit [22]. For the four-core die used here, die swell causes distortion of the preform, impacting features such as the wall-thickness, core-size, and strut formation. This is pronounced due to the different feature sizes, which then have different flow speeds at the die exit. For example, the die exit used for Fig. 1(d) has outer wall, core diameter, and strut thicknesses of 1.03, 3.28, and 0.63 mm, respectively.

A complex internal die geometry and die exit, made possible with 3D printing, can be designed to compensate the distortion. For example, in Fig. 1(b) the glass flow was significantly faster for the cores compared to the outer wall, resulting in die swell and associated deformations. The preform in Fig. 1(c) is the result of balancing the flow of glass between the outer wall and the cores throughout the internal structure of the die. In this case there was insufficient glass reaching the struts, which was rectified by increasing the strut thickness in the die used to produce the preform shown in Fig. 1(d).
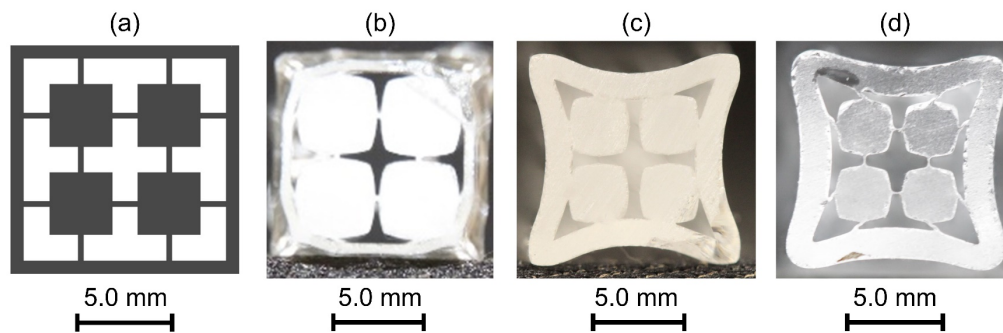

Fig. 1. (a) Target preform design (black is glass, white is air). (b-d) Cross sectional images of the extruded four-core preforms. (b) Initial attempt resulting in significant die swell of the cores, extruded through a die with exit design shown in Fig. 1(a). (c) Preform result after balancing the glass flow between the outer wall and the cores, but which failed to form struts. (d) Preform result after increasing the strut thickness in the die design relative to Fig. 1(c).

2.2 Fiber drawing

The preform from Fig. 1(d) was caned to 1.0 mm diameter using a fiber draw tower and then stacked in a 5 × 5 rectangular arrangement, as shown in Fig. 2(a). The process of drawing to cane led to the outer cross section shape forming close to a square outer geometry compared to the original preform, allowing it to be stacked into a rectangular configuration.

The 5 × 5 assembly was joined and sealed at one end using a two-part epoxy and joined at the opposite end using a silica-based high temperature adhesive (Resbond 940 LE). The 5 × 5 assembly was then inserted into an extruded lead-silicate (F2) tube with square inner structure (5.5 mm × 5.5 mm) and round outer structure (diameter of 12 mm), with cross section shown in Fig. 2(b). The ability to use a square inner shape for the tube, made possible through extrusion, meant that the stacked assembly shape could be matched closely to the tube. The epoxied end of the 5 × 5 assembly was located at the top of the square-inner tube, which acted as a seal for self-pressurization of the individual canes during the draw and acted as a support to hang the assembly in the tube. The preform was then drawn into optical fiber with an outer diameter of 160 μm, as shown in Fig. 2(c). It can be seen that self-pressurization of the individual canes successfully closed the gap between adjacent canes. The diameter of each core was measured to be 3.1 μm ± 0.3 μm (one standard deviation), while the average pitch between cores over the structured region of the fiber was measured to be 7.6 μm.
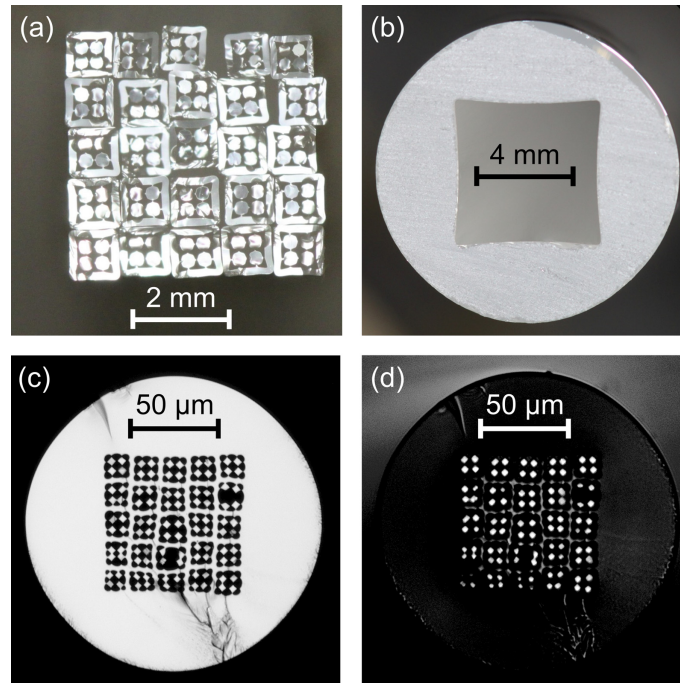
Fig. 2. (a) Stacked array of canes that were drawn from the preform shown in Fig. 1(d). (b) Extruded tube with square inner, which was designed to allow the stacked assembly in Fig. 2(a) to be inserted. (c) Drawn fiber with reflection mode microscope image. (d) Drawn fiber with transmission mode microscope image.

A small piece of the imaging MOF was coated with marker pen to strip cladding modes and viewed under an optical microscope with transmission illumination, shown in Fig. 2(d). It is clearly seen that the majority of the individual cores of the fiber can support guided light that is independent of the cladding.

3. Optical experiments

Three different optical experiments have been performed to characterize the imaging MOF. The experimental setups that were used are shown in Fig. 3. Note that in each experiment the imaging MOF was covered with at least 200 mm of absorbing carbon paste in order to strip cladding modes. This also has the effect of removing light from the borders of each 2×2 array in the fiber as these are optically connected to the cladding.

(a) Single core transmission
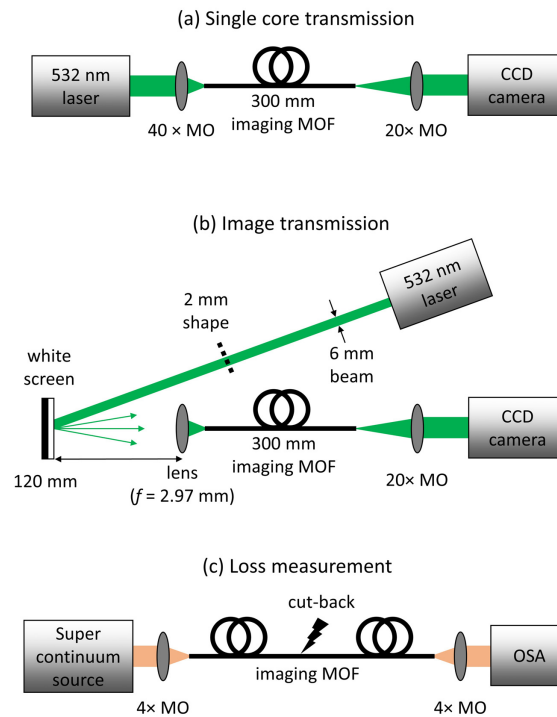
(b) Image transmission

(c) Loss measurement

Fig. 3. Optical experimental configurations for testing the imaging MOF. (a) Transmission through a single core of the imaging MOF. (b) Transmitting the image of simple geometric shapes through the imaging MOF. (c) Loss measurement through the imaging MOF, averaged over all cores of the fiber. MO is microscope objective, OSA is optical spectrum analyzer.

The first experiment [setup in Fig. 3(a)] was designed to test the ability of individual cores in the imaging MOF to independently guide light. A 532 nm laser beam was focused onto the end face of a 300 mm long piece of imaging MOF using a 40 × microscope objective. The focused light was coupled into a single core and the output of the fiber was imaged onto a CCD camera (Ophir-Spiricon, SP300) using a 20 × microscope objective. Figure 4(a) shows the cross-section of the imaging MOF and the dashed lines show the sections of the fiber tested as examples. In Figs. 4(b) to 4(d) the light was coupled to a single core and the corresponding output shows a single illuminated core. For a small number of cores the struts to adjacent cores are relatively thicker [1.2 μm for the example in Fig. 4(e)], and there is coupling between cores as evident in the transmitted image in Fig. 4(e).

The second experiment [setup in Fig. 3(b)] was designed to show that an image can be coherently transported from one end of the fiber to the other. A 532 nm laser bean was expanded to approximately 6 mm in diameter using two lenses (focal lengths of 30 mm and 200 mm). The expanded beam was then passed through different simple image templates (uniform illumination, square, and annulus), with diameters of approximately 2 mm, and directed to a white screen. A 2.97 mm focal length lens was then placed 120 mm from the white screen and used to image the patterns with diameters the order of 50 μm onto the end face of a 300 mm long piece of imaging MOF. The fiber output was imaged onto a CCD camera using a 20 × microscope objective with the resulting images shown in Figs. 5(a) to 5(c).
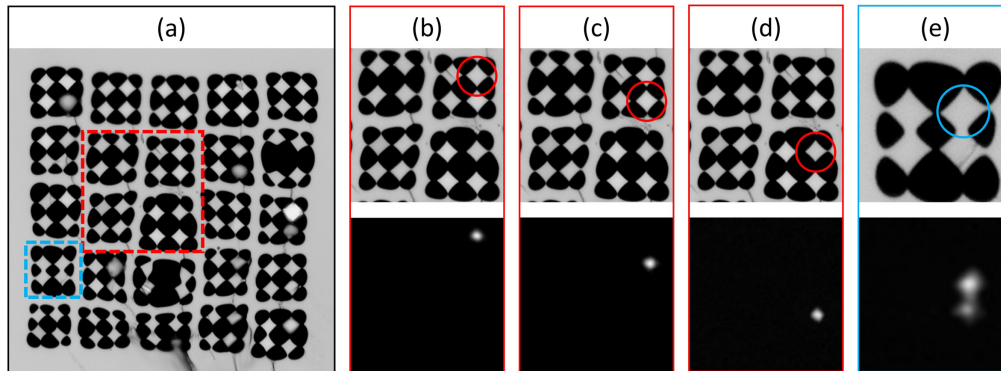
Fig. 4. (a) Reflected microscope image of the imaging MOF, same image as shown in Fig. 2(c). (b-d) Upper images show a zoomed microscope image of the fiber and the circles show the locations where the 532 nm laser beam was focused onto the fiber. The lower images show the corresponding transmitted images recorded on the camera, showing propagation through a single core without coupling to adjacent cores. (e) The laser beam was focused on a core with relatively thicker strut to an adjacent core (approx. 1.2 μm). In this case coupling to the adjacent core was observed in the transmitted image.

While the results in Fig. 5 show that the fill-factor could be improved and that not all pixels are equally bright, it is seen that coherent images can be successfully transported through the imaging MOF. The fill-factor and resolution is directly a result of the fabricated fiber. In Sec. 4 theoretical calculations will give an estimate of the ultimate resolution limit for an imaging MOF using lead-silicate glass. The non-uniform pixel brightness, as best seen for the case of uniform illumination [Fig. 5(a)] and with a histogram shown in Fig. 5(d), is due to a combination of factors. This includes non-uniform cleaving of the input and output end of the imaging MOF, strut breakage for some cores in the fiber that formed during the fiber draw [see Fig. 4(a)], multimode interference within each imaging MOF core, the Gaussian transverse shape of the expanded laser beam, and laser speckle on the illuminated screen.
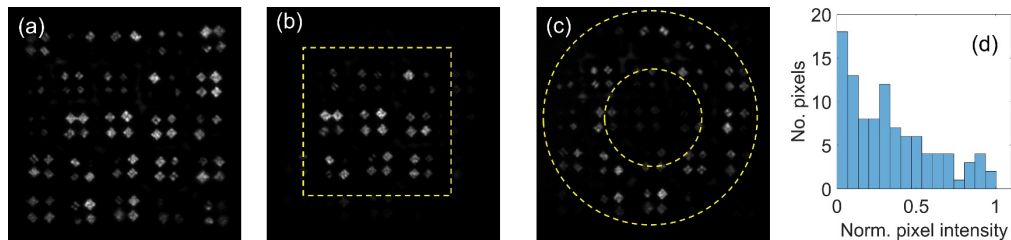

Fig. 5. Patterns transmitted through the imaging MOF. (a) Uniform illumination. (b) Square. (c) Annulus. Yellow dashed lines show the approximate position and orientation of the imaged shapes. (d) Histogram showing the pixel (core) intensity distribution for the uniform illumination image in Fig. 5(a).

The third experiment [setup in Fig. 3(c)] was used to test the transmission loss of the imaging MOF. The output of a super continuum source (NKT Photonics, SuperK Extreme) was focused onto the end face of a 5 m long imaging MOF using a 4 × microscope objective, with approximately uniform illumination across the fiber cores. The output of the fiber was directed to an optical spectrum analyzer and recorded over a wavelength range from 600 to 1600 nm. The fiber was cut-back in 1 m segments and the spectrum recorded for each. The optical loss was then determined as the change in transmitted power versus fiber length and the results are shown in Fig. 6.

The loss varies between 2.5 to 5.5 dB/m across the measured wavelength range. It is observed that the imaging MOF loss is higher compared to the bulk material loss. This may

be due to factors such as stresses from the multiple thermal cycles involved in extrusion and fiber drawing (noting that the preform and canes were not annealed), environmental contamination of the preform and canes, or contamination from the 3D titanium printed die. These effects can be minimized in the future and the fiber can nevertheless be used at meter-scaled lengths, depending on the intended application.
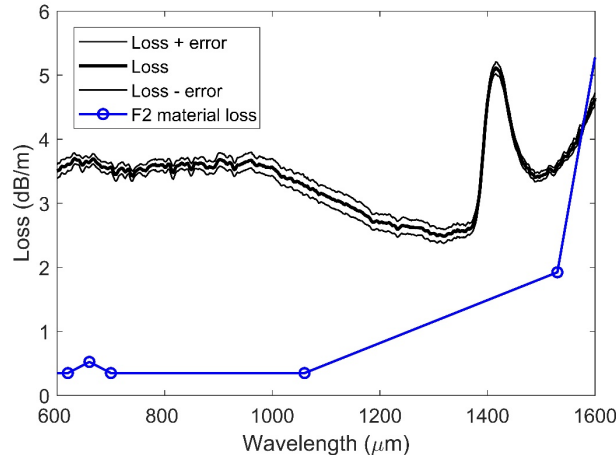

Fig. 6. Transmission loss of the imaging MOF when coupled uniformly across all cores (black curve). Blue data points represent the material loss provided by the manufacturer for F2 lead-silicate glass (Schott). https://www.schott.com/advanced_optics/us/abbe_datasheets/schott-datasheet-f2.pdf

4. Calculation on resolution limit

A key requirement for an imaging fiber is that cross-talk between individual cores is minimized. We have used a simplified model of two square cores with a width and height ("core diameter") of D, and a separation of S. The model was implemented using commercial finite element method software (COMSOL v5.2). Such a two-core fiber, when the two cores are identical, supports even and odd nondegenerate mode solutions for each polarization [Fig. 7(a)]. The values of D and S were varied to determine the coupling length, L_c, for coupling between the even and odd modes, where the coupling length is calculated by [23]:

$$L_c = \frac{\lambda}{2(n_{eff}^e - n_{eff}^o)},$$

(1)

λ is the free space wavelength and n_{eff} is the effective index of the even (e) and odd (o) modes. Equation (1) can be understood intuitively that the closer and/or smaller the cores are then the greater the optical field interaction between the two cores, leading to increasing difference in effective index and a decrease in the coupling length.

Figure 7(b) shows the values for core diameter and core separation for three values of the coupling length (0.1 m, 1.0 m and 10 m), at a wavelength of 532 nm, and considering the x-polarization as defined in Fig. 7(a). The dashed lines show values for various fill factors (fraction of glass versus total cross-sectional area). For example, if a core diameter of 1.2 μm is used then the cores must be separated by 0.60 μm to have a coupling length of at least 1.0 m, in which case the fill factor is just below 45%. This would allow for approximately 3,800 pixels in a 125 μm fiber or 15,000 pixels in a 250 μm fiber.

This calculation can be considered a worst-case scenario as it is difficult to fabricate an imaging fiber with identical cores. Any imperfection in the core size or geometry will significantly suppress the coupling between the cores allowing a higher pixel density [23,24].
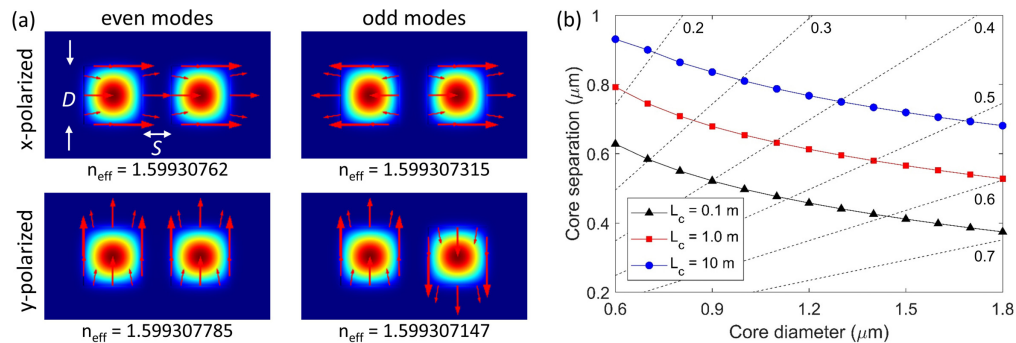
Fig. 7. (a) Geometry of the numerical model showing both the even and odd modes and the two polarizations for the example case of core diameter, D, being 1.2 µm and the separation, S, being 0.6 µm. (b) Values of core diameter and core separation that give coherence lengths of 0.1 m, 1.0 m and 10 m. Labelled dashed lines show the pixel fill factor as a fraction.

5. Discussion and conclusions

We have demonstrated the proof-of-concept fabrication of a soft-glass imaging microstructured optical fiber. The optical fiber preform was fabricated via extrusion through a 3D printed titanium die. The preform was then caned, stacked and redrawn into a 100 core fiber. The use of 3D printing and extrusion combined with stacking allows for unprecedented control of the preform and fiber geometry, such as the rectangular features in this work. Optical experiments confirm that the cores independently guide light and that the fiber allows for the coherent transmission of simple geometric shapes through the fiber.

Theoretical calculations on the coupling length between two adjacent cores show that the fabricated fiber core and core-separation dimensions are significantly larger than required for image transmission. It is theoretically possible to reduce the pixel pitch to the order of 1.8 µm. Therefore our future work will focus on attaining these dimensions and also increasing the total pixel count by 1-2 orders of magnitude. This could be achieved by a combination of increasing the number of cores in the extrusion die design and also stacking a greater number of canes within the final preform assembly. Note that for the extrusion die design used here we are close to the feature size limit (strut widths) through which glass can be successfully extruded (currently 0.64 mm compared to a limit of approximately 0.4 mm). Therefore the maximum core array that could be made using the current 30 mm diameter glass billet would be 3 × 3. By increasing the glass billet diameter to 50 mm a 5 × 5 core array could be fabricated.

Ultimately we envisage that glass-based imaging microstructured optical fibers would find use in applications such as in-vivo white-light and spectroscopic imaging. Of particular interest would be spectroscopic imaging through the use of mid-infrared transmitting glasses, such as chalcogenide or fluoride glasses.

References

1. C. M. Lee, C. J. Engelbrecht, T. D. Soper, F. Helmchen, and E. J. Seibel, "Scanning fiber endoscopy with highly flexible, 1 mm catheterscopes for wide-field, full-color imaging," J. Biophotonics **3**(5-6), 385–407 (2010).

2. I. N. Papadopoulos, S. Farahi, C. Moser, and D. Psaltis, "High-resolution, lensless endoscope based on digital scanning through a multimode optical fiber," Biomed. Opt. Express **4**(2), 260–270 (2013).
3. R. N. Mahalati, R. Y. Gu, and J. M. Kahn, "Resolution limits for imaging through multi-mode fiber," Opt. Express **21**(2), 1656–1668 (2013).
4. M. Plöschner, T. Tyc, and T. Čižmár, "Seeing through chaos in multimode fibres," Nat. Photonics **9**(8), 529–535 (2015).
5. D. E. Boonzajer Flaes, J. Stopka, S. Turtaev, J. F. de Boer, T. Tyc, and T. Čižmár, "Robustness of light-transport processes to bending deformations in graded-index multimode waveguides," Phys. Rev. Lett. **120**(23), 233901 (2018).
6. S. Qi, B. Zhang, C. Zhai, Y. Li, A. Yang, Y. Yu, D. Tang, Z. Yang, and B. Luther-Davies, "High-resolution chalcogenide fiber bundles for longwave infrared imaging," Opt. Express **25**(21), 26160–26165 (2017).
7. T. M. Monro and H. Ebendorff-Heidepriem, "Progress in microstructured optical fibers," Annu. Rev. Mater. Res. **36**(1), 467–495 (2006).
8. M. van Eijkelenborg, "Imaging with microstructured polymer fibre," Opt. Express **12**(2), 342–346 (2004).
9. J. Wang, X. Yang, and L. Wang, "Fabrication and experimental observation of monolithic multi-air-core fiber array for image transmission," Opt. Express **16**(11), 7703–7708 (2008).
10. S. C. Warren-Smith, H. Ebendorff-Heidepriem, T. C. Foo, R. Moore, C. Davis, and T. M. Monro, "Exposed-core microstructured optical fibers for real-time fluorescence sensing," Opt. Express **17**(21), 18533–18542 (2009).
11. G. Tsiminis, K. J. Rowland, E. P. Schartner, N. A. Spooner, T. M. Monro, and H. Ebendorff-Heidepriem, "Single-ring hollow core optical fibers made by glass billet extrusion for Raman sensing," Opt. Express **24**(6), 5911–5917 (2016).
12. H. Ebendorff-Heidepriem, S. C. Warren-Smith, and T. M. Monro, "Suspended nanowires: fabrication, design and characterization of fibers with nanoscale cores," Opt. Express **17**(4), 2646–2657 (2009).
13. E. P. Schartner, G. Tsiminis, A. François, R. Kostecki, S. C. Warren-Smith, L. V. Nguyen, S. Heng, T. Reynolds, E. Klantsataya, K. J. Rowland, A. D. Abell, H. Ebendorff-Heidepriem, and T. M. Monro, "Taming the light in microstructured optical fibers for sensing," Int. J. Appl. Glass Sci. **6**(3), 229–239 (2015).
14. T. M. Monro, S. Warren-Smith, E. P. Schartner, A. François, S. Heng, H. Ebendorff-Heidepriem, and S. Afshar, "Sensing with suspended-core optical fibers," Opt. Fiber Technol. **16**(6), 343–356 (2010).
15. S. Afshar V, W. Q. Zhang, H. Ebendorff-Heidepriem, and T. M. Monro, "Small core optical waveguides are more nonlinear than expected: experimental confirmation," Opt. Lett. **34**(22), 3577–3579 (2009).
16. H. Ebendorff-Heidepriem, J. Schuppich, A. Dowler, L. Lima-Marques, and T. M. Monro, "3D-printed extrusion dies: a versatile approach to optical material processing," Opt. Mater. Express **4**(8), 1494–1504 (2014).
17. X. Jiang, F. Babic, J. Huang, S. Xie, Z. Wang, R. Sopalla, N. Joly, and P. S. J. Russell, "Recent advances in fabrication and applications of nanostructured soft-glass optical fibres," Advanced Photonics Congress, SoM2H.2 (2018).
18. X. Jiang, N. Y. Joly, R. Sopalla, F. Babic, J. Huang, and P. S. J. Russell, "Soft glass microstructured fibers and their applications," Advanced Photonics Congress, SoW3G.1 (2016).
19. J. Y. Y. Leong, S. Asimakis, F. Poletti, P. Petropoulos, X. Feng, R. C. Moore, K. E. Frampton, T. M. Monro, H. Ebendorff-Heidepriem, W. H. Loh, and D. J. Richardson, "Nonlinearity and dispersion control in small core lead silicate holey fibers by structured element stacking," Proc. Optical Fiber Communication Conference, OTuH1 (2006).
20. J. Y. Y. Leong, S. Asimakis, F. Poletti, P. Petropoulos, X. Feng, R. C. Moore, K. E. Frampton, T. M. Monro, H. Ebendorff-Heidepriem, W. H. Loh, and D. J. Richardson, "Towards zero dispersion highly nonlinear lead silicate glass holey fibres at 1550nm by structured-element-stacking," Proc. European Conference on Optical Communication, Th4.4.5 (postdeadline) (2005).
21. H. Ebendorff-Heidepriem and T. M. Monro, "Analysis of glass flow during extrusion of optical fiber preforms," Opt. Mater. Express **2**(3), 304–320 (2012).
22. H.-J. Mayer, C. Stiehl, and E. Roeder, "Applying the finite-element method to determine the die swell phenomenon during the extrusion of glass rods with non-circular cross-sections," J. Mater. Process. Technol. **70**(1-3), 145–150 (1997).
23. K. L. Reichenbach and C. Xu, "Numerical analysis of light propagation in image fibers or coherent fiber bundles," Opt. Express **15**(5), 2151–2165 (2007).
24. X. Chen, K. L. Reichenbach, and C. Xu, "Experimental and theoretical analysis of core-to-core coupling on fiber bundle imaging," Opt. Express **16**(26), 21598–21607 (2008).